ACS APPLIED MATERIALS & INTERFACES

Research Article

www.acsami.org

Effects of Ni Doping on the Initial Electrochemical Performance of Vanadium Oxide Nanotubes for Na-Ion Batteries

Hyunjin Kim, Ryoung-Hee Kim, Seok-Soo Lee, Yongsu Kim, Dong Young Kim, and Kwangjin Park*

Samsung Advanced Institute of Technology (SAIT), Electronic Materials Research Complex, 130, Samsung-ro, Maetan-dong, Yeongtong-gu, Suwon-si, Gyeonggi-do 443-803, Republic of Korea

Supporting Information

ABSTRACT: In this study, we demonstrated the intercalation of Na in hydrothermally synthesized VO_x nanotubes (NTs) and Ni-doped VO_x NTs. The changes induced in the structures of the two nanomaterials during the Na intercalation process were investigated through X-ray diffraction (XRD) analyses. It was observed that the initial capacity and rate performance of the Ni-doped VO_x NTs were improved. The results of X-ray photoelectron spectroscopy (XPS) and conductance measurement confirmed that higher initial capacity and rate performance were attributed to an increase in the valence states of vanadium and increased conductivity after the Ni exchange process.

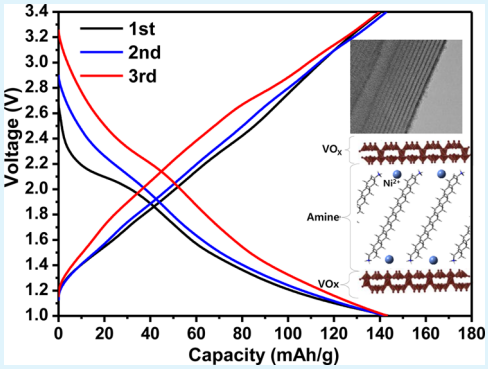

KEYWORDS: *vanadium oxide, nanotubes, Na battery, hydrothermal synthesis, Ni doping, cationic exchange*

1. INTRODUCTION

Li-ion batteries are widely used in numerous applications and devices, including electric vehicles and energy storage systems.[1−3] However, Li is a limited resource, and there is an urgent need to discover alternative materials for next-generation batteries. Recently, Na-ion batteries have started attracting attention as alternatives to Li-ion batteries, owing to the abundance of Na and the relatively low manufacturing cost of Na-ion batteries.

Over the past few decades, much progress has been in the development of cathode materials for Na-ion batteries. Layered transition metal oxides such as Na_xMO_2 (M = Co, Ni, Cr, Fe, Mn) have emerged as suitable active cathode materials for Na-ion batteries.[1−6] Because the volume of the Na ion is approximately 70% higher than that of the Li ion, a larger open framework is required in the case of the former. Among the Na_xMO_2 materials being explored, vanadium oxide, which has a layered structure that should facilitate mobile cation insertion and extraction within the structure, seems one of the most promising.[7−9] It is known that vanadium oxide, which has a large *d*-spacing, exhibits good electrochemical performance when used for cathodes in Li-ion and Na-ion batteries. Hamani et al. and Tepavcevic et al. attempted to improve the characteristics of vanadium oxide for use as a cathode material in Na-ion batteries.[7,8] Recently, Su and Wang reported that the electrochemical performance Na-ion batteries could be improved by using bilayered V_2O_5 that was structured in the form of nanobelts.[9] Moreover, vanadium oxide materials structured in the form of nanosheets,[10] nanobelts,[11] and nanoribbons[12] exhibit improved electrochemical performances, as they have higher surface areas and short ion-migration pathways. Among these nanostructured vanadium oxide materials, vanadium oxide nanotubes (VO_x NTs), which have an open-ended and multiwalled tubular structure, show a lot of promise as they have a large active surface area and numerous channels for ionic transport.[13−18] However, VO_x NTs exhibit high capacity-fading rates. This is probably because of the lower valence of vanadium in the material and the existence of the amine templates, which are used to fabricate the NTs, in a large amount. Cationic metal doping through an exchange reaction seems to be a promising technique for overcoming this issue.[14−17]

In this study, we fabricated VO_x NTs using V_2O_5 as a precursor and an amine as the template to control the morphology of the NTs. Further, by the exchanging organic amine templates with Ni cations, we were able to dope Ni within the walls of the VO_x NTs. Na intercalation was achieved in the VO_x NTs and the Ni-doped VO_x NTs. The enhanced initial capacity and rate performance from the Ni-doped VO_x NTs were attributed to higher valence states of vanadium and increased conductivity of the Ni-doped VO_x NTs.

2. RESULTS AND DISCUSSION

Transmission electron microscopy (TEM) was employed to characterize the structures of the synthesized samples. The insets of Figure 1a and b show TEM images of the VO_x NTs

Received: April 23, 2014
Accepted: June 24, 2014
Published: June 24, 2014

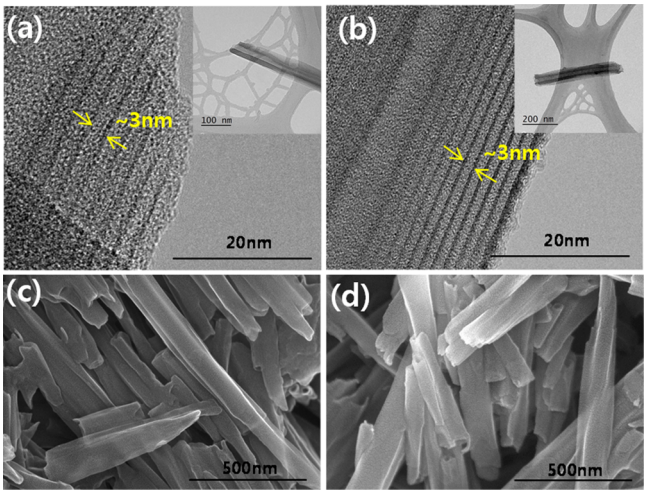

Figure 1. (a) Low-resolution TEM image of the VO_x NTs (inset is an HRTEM image) and (b) low-resolution TEM image of the Ni-doped VO_x NTs (inset is a HRTEM image). SEM images of the (c) VO_x NTs and (d) Ni-doped VO_x NTs.

and the Ni-doped VO_x NTs. Both samples had an open-ended, multilayered tubular structure, with the outer diameter being approximately 100 nm. The high-resolution (HR) TEM images in Figure 1a and b show that the Ni-doped VO_x NTs had a layered structured that was composed of alternately arranged VO_x layers (dark fringes), which had a thickness of ~0.7 nm, and amine layers (broad and light fringes), which had a thickness of ~2 nm. Even after the cation exchange process, the multiwalled tubular structure of the VO_x NTs remained intact. In the HRTEM images, the dark and light fringes represent the VO_x layers and the octadecylamine ($CH_3(CH_2)_{16}CH_2NH_2$) templates, respectively. High- and low-magnification scanning electron microscopy (SEM) images of the VO_x NTs and the Ni-doped VO_x NTs are shown in Figure 1c and d. There was no significant difference in the morphologies of the VO_x NTs and the Ni-doped VO_x NTs, indicating that the overall morphology of the VO_x NTs remained almost unchanged after the cation exchange process.

Schematics of the VO_x NTs and the Ni-doped VO_x NTs are shown in Figure 2a. The VO_x NTs contained the amine templates.[19] During the cationic exchange process, the protonated amine species are either partially replaced by Ni cations or Ni cations are inserted at the interface between the layered VO_x and the protonated amine templates, resulting in a decrease in the interlayer spacing. The structures of the two samples were also investigated through X-ray diffraction (XRD) analyses. Figure 2b shows the diffraction peaks of the VO_x NTs and the Ni-doped VO_x NTs. The sharp peak in the small-angle region extending from 3° to 15° corresponded to the well-ordered, layered structure of the tubular VO_x NTs, and the diffraction peaks in the large-angle region extending from 15° to 50° corresponded to the two-dimensional structure of the VO_x layers. Owing to the direct reflection of the X-ray beam, we have only considered data corresponding to $2\theta > 3°$. The first peak noticed in the XRD patterns was the (002) peak attributable to the layered structure of both the VO_x NTs and the Ni-doped VO_x NTs. The peak in the case of the Ni-doped VO_x NTs was slightly shifted toward the higher-angle region, indicating that the interlayer spacing in this case was lower. The interlayer spacing calculated from the XRD patterns was 3.4 nm for the VO_x NTs and 3.3 nm for the Ni-doped VO_x NTs. These

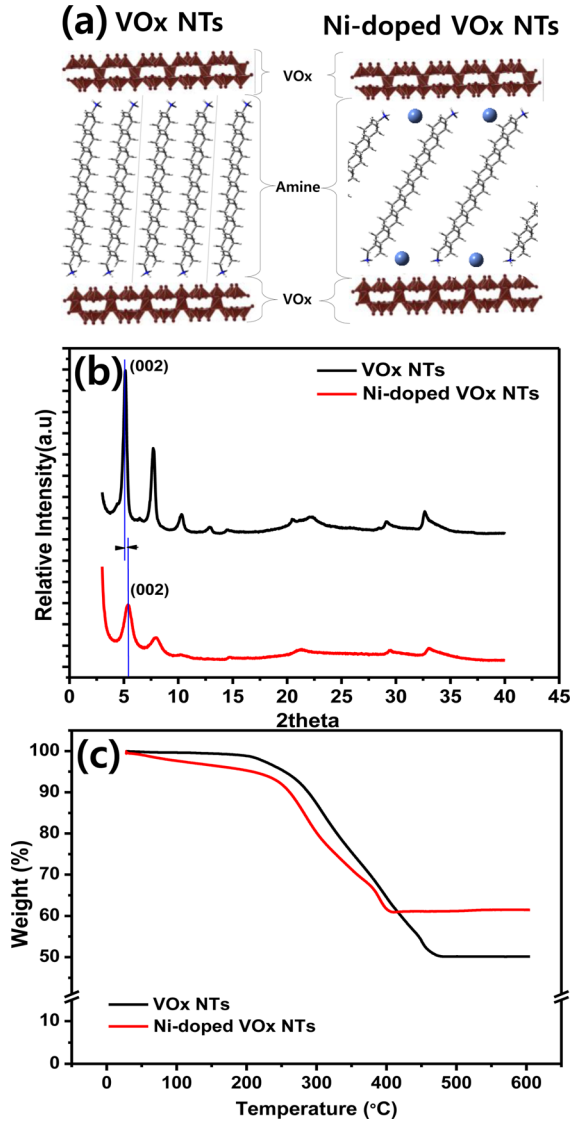

Figure 2. (a) Schematic illustration of the VO_x NTs and Ni-doped VO_x NTs. (b) XRD patterns of the VO_x NT and Ni-doped VO_x NT powders. (c) TGA curves of the VO_x NTs and the Ni-doped VO_x NTs.

results were also confirmed through small-angle X-ray scattering (SAXS) analysis, as shown in the Supporting Information. The full widths at half-maximum (FWHMs) of the XRD peaks of the Ni-doped VO_x NTs were greater than those of the peaks of the VO_x NTs, indicating that the distribution of the interlayer spacing was broader in the case of the Ni-doped VO_x NTs. Moreover, the positions of the (hk0) diffraction peaks in the high-angle region were the same for both the samples,[19] indicating that the cation exchange reaction did not have an effect on the two-dimensional structure of the VO_x layers.

Thermogravimetry (TG) measurements were made to determine the concentration of the organic templates in the fabricated samples. The temperature was increased from room temperature to 550 °C during the TG measurements. Weight losses of 50% and 40% were observed for the VO_x NTs and the Ni-doped VO_x NTs, respectively, as shown in Figure 2c; these values were reflective of the percentage concentration of the organic templates. The organic templates were initially present

in the VO_x NTs in a larger quantity than the case for the Ni-doped VO_x NTs, indicating that a small proportion of the organic templates was exchanged with the Ni cations during the cationic exchange reaction.

Table 1 shows the concentrations of the constituent elements in the VO_x NTs and the Ni-doped VO_x NTs. The

Table 1. Molar Concentrations of Elements in VO_x and Ni-Doped VO_x NTs

	mole ratio, %					
sample	C	H	N	V	Ni	O
VO_x	0.261	0.555	0.010	0.045	0.000	0.129
Ni-doped VO_x	0.224	0.502	0.007	0.062	0.006	0.198

concentrations of V and Ni were determined using inductively coupled plasma atomic emission spectroscopy (ICP-AES), which was performed on a Shimadzu ICPS-8100 sequential spectrometer, while those of the elements forming the organic compounds (i.e., C, H, N) were determined using an elemental analyzer (PE 2400 Series II). We found that V and Ni was present in the VO_x NTs in a molar ratio of 10:1 (V:Ni). In addition, the concentrations of C, H, and N in the Ni-doped VOx NTs were 11% lower than their concentrations in the VO_x NTs. This also indicated that a small proportion of the amine templates had been replaced by Ni cations. It can thus be surmised that the Ni cations were effectively interchanged with the protonated amine templates through the cationic exchange reaction, with the cations being positioned in the space between the VO_x layers, as described in Figure 2a. The electrical conductivities of VO_x and Ni-VO_x NTs were 9.225×10^{-7} and 1.329×10^{-6} S cm^{-1}, respectively. The higher conductivity of Ni-VO_x NTs is because organic amine species are partly replaced by metallic Ni during exchange reaction.

Figure 3a and b shows the potential versus capacity profiles of the VO_x NTs and the Ni-doped VO_x NTs during the 1st, 2nd, 3rd, 5th, and 10th cycles at 0.1C. The charging/discharging profiles of the VO_x NTs and the Ni-doped VO_x NTs were similar. The first discharging capacity of the VO_x NTs was 110 mA h g^{-1}, and that of the Ni-doped VO_x NTs was 140 mA h g^{-1}; thus, there was an increase of 30 mA h g^{-1} after the doping with Ni. This increase in capacity might be due to the participation of Ni in the electrochemical process. The potentials of both the VO_x NTs and the Ni-doped VO_x NTs plateaued at approximately 2.1 V in the first discharging profile. This plateau at 2.1 V corresponds to Na ions being inserted into the lattice framework of the VO_x NTs; a similar phenomenon has been reported in the case of tunnel-structured vanadium-based cathode materials as well.[9] However, the second discharging profile of the VO_x NTs did not exhibit a voltage plateau, supposedly because of structural degradation of VO_x interlayers and increased overpotential during cycling. On the other hand, the profile of the Ni-doped VO_x NTs still showed a voltage plateau at a voltage slightly higher than 2.1 V during cycling, indicating clearly that the intercalation process was still dominant. Up to the third cycle, the shape of the discharge graph for the Ni-doped VO_x NTs and the voltage corresponding to the potential plateau were similar to those corresponding to the first cycle. Moreover, the efficiency of the Ni-doped VO_x NTs was much higher; the Ni-doped VO_x NTs exhibited an efficiency of 99% during the first and second cycles. This indicates that the intercalated Na cations were completely extracted from the Ni-doped VO_x NTs-based

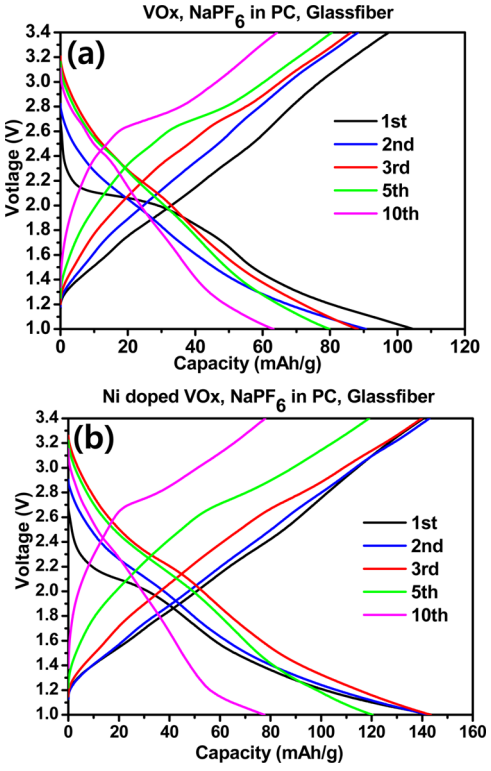

Figure 3. Discharge and charge profiles of (a) the VO_x NTs at 0.1C and (b) the Ni-doped VO_x NTs at 0.1C.

cathode. However, after the third cycle, the charge/discharge curves of the Ni-doped VO_x NTs become similar to those of the VO_x NTs, exhibiting capacity fading.

One of the most important characteristics of a cathode material to be used in energy storage systems is its rate capability. The rate capabilities of the VO_x NTs and the Ni-doped VO_x NTs were tested using cells that were cycled at 0.1C, 0.2C, 0.5C, and 1C. Figure 4a and b shows the potential versus capacity profiles of the VO_x NTs and the Ni-doped VO_x NTs for the different C-rates. The potential plateaus in the discharging and charging profiles at a C-rate of 0.1C were located at 2.1, and 3.0 V, respectively. With an increase in the C-rate, the potential plateaus of both samples disappeared. Figure 4c shows the capacities of the two materials for the various C-rates. As the C-rate was increased, the capacities of both samples decreased. This can be ascribed to an increase in the overpotential resulting from the fact that there was not enough time for the intercalation of the Na cations into the crystal lattice.[7] It was found that the Ni-doped VO_x NTs exhibited a charging/discharging capacity that was approximately 40 mA h g^{-1} higher than that of the VO_x NTs for the entire range of the C-rates. The capacities of both samples were measured again after the C-rate was reduced to the original value (0.1C). The capacity of the Ni-doped VO_x NTs recovered to up to 71% of their original capacity, while that of the VO_x NTs recovered to 55% of its original value. This indicated that the Ni-doped VO_x NTs were structurally much robust than the bare VO_x NTs. The improved rate performance of Ni-doped VO_x NTs is attributed to higher electrical conductance of Ni-doped VO_x than bare VO_x NTs. Figure 4d shows the discharge/charge capacities of the two materials as functions of the number of cycles for a C-rate of 0.1C. It can be

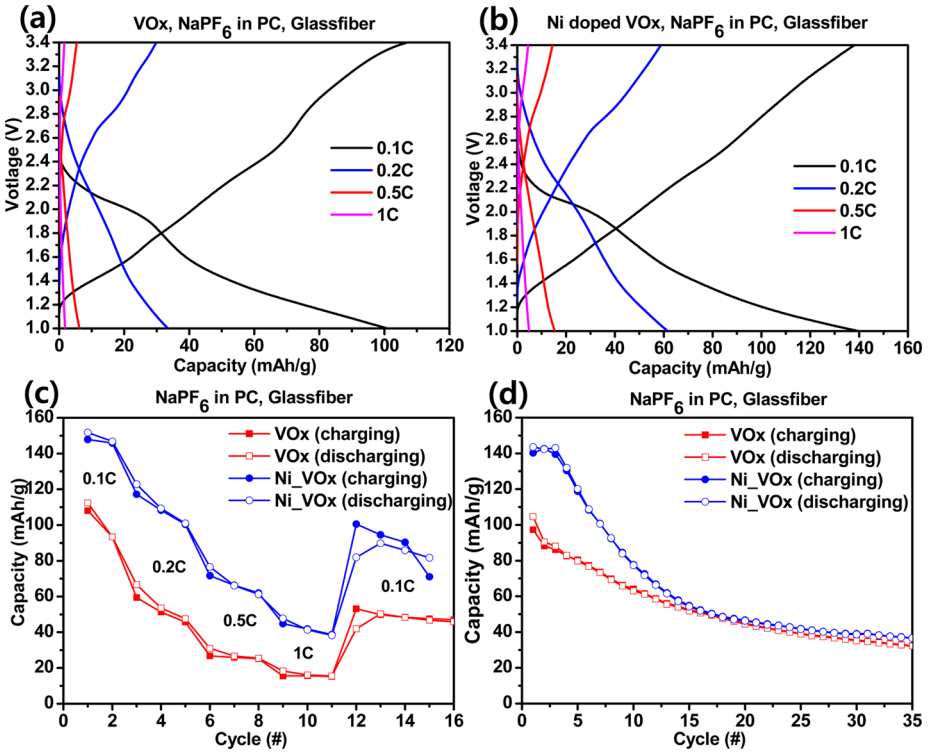

Figure 4. Discharge and charge profiles of (a) the VO_x NTs and (b) the Ni-doped VO_x NTs at different C-rates. (c) Rate performances of the VO_x NTs and the Ni-doped VO_x NTs at the different C-rates. (d) Discharge/charge capacities of the materials vs the number of cycles at 0.1C.

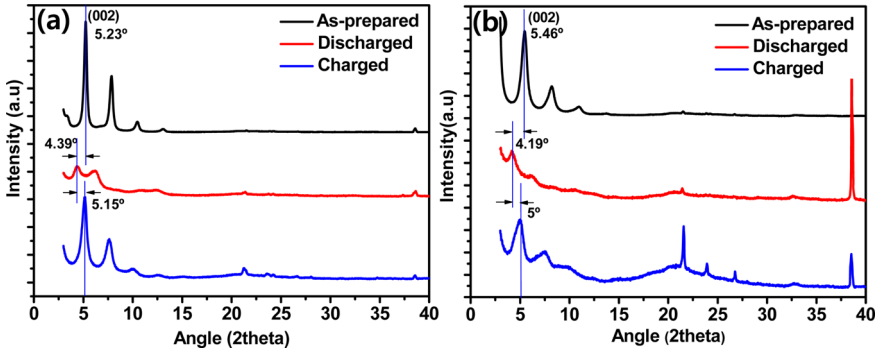

Figure 5. XRD spectra of the as-prepared, after-first-discharge, and after-first-charge electrodes of the (a) VO_x NTs and (b) Ni-doped VO_x NTs.

seen clearly that the initial capacity of the Ni-doped VO_x NTs was much higher that of the VO_x NTs.

The changes in the structures of the VO_x NTs and the Ni-doped VO_x NTs during the electrochemical Na intercalation process were investigated through XRD analyses. The XRD spectra were taken with three different electrochemical stages: (1) as-prepared electrodes, (2) the electrode after the cells is fully discharged up to 1 V, and (3) the electrode after the cell is fully charged up to 3.4 V. The XRD spectra of the as-prepared, discharged, and charged electrodes of the two materials are shown in Figure 5. The low-angle diffraction peak (i.e., the (002) peak) of the as-prepared VO_x NTs (Ni-doped VO_x NTs) were positioned at 5.23° (5.46°) and corresponded to an interlayer spacing of 3.3 nm (3.2 nm). After the first discharge, the low-angle XRD peaks of both materials slightly shifted to a lower angle: 4.39° for VO_x NTs and 4.19° for Ni-doped VO_x NTs; these values corresponded to an interlayer spacing of 4.05 nm for the VO_x NTs and 4.21 nm for the Ni-doped VO_x NTs. After the first charge, the XRD peak shifted back to a higher angle: 5.15° (interlayer spacing of 3.43 nm) for the VO_x NTs and 5° (interlayer spacing of 3.53 nm) for the Ni-doped VO_x NTs. This indicated that, with the discharging process, the interlayer spacing of both the VO_x NTs and the Ni-doped VO_x NTs increased to values greater than those corresponding to the initial and charged states. This effect can be ascribed to the insertion of Na cations during the intercalation process.

To elucidate the role of Ni in causing the initial capacity of the Ni-doped VO_x NTs to be higher, we analyzed the chemical states of the VO_x NTs and the Ni-doped VO_x NTs using X-ray photoelectron spectroscopy (XPS). Figure 6 shows the V $2p_{3/2}$ and Ni 2p core-level spectra of the two samples. As shown in Figure 6a and b, after background subtraction, the V spectra consisted of two components, namely, peaks at 516 and ~517.3 eV, which corresponded to V^{4+} and V^{5+} ions, respectively.[20] The V^{4+}/V^{5+} ratio for the VO_x NTs was 1:0.94, while that for the Ni-doped VO_x NTs was 1:2, indicating that the vanadium ions were oxidized during cationic exchange reaction. The higher valences of vanadium ions in the Ni-doped VO_x NTs

dx.doi.org/10.1021/am502480v | ACS Appl. Mater. Interfaces 2014, 6, 11692−11697

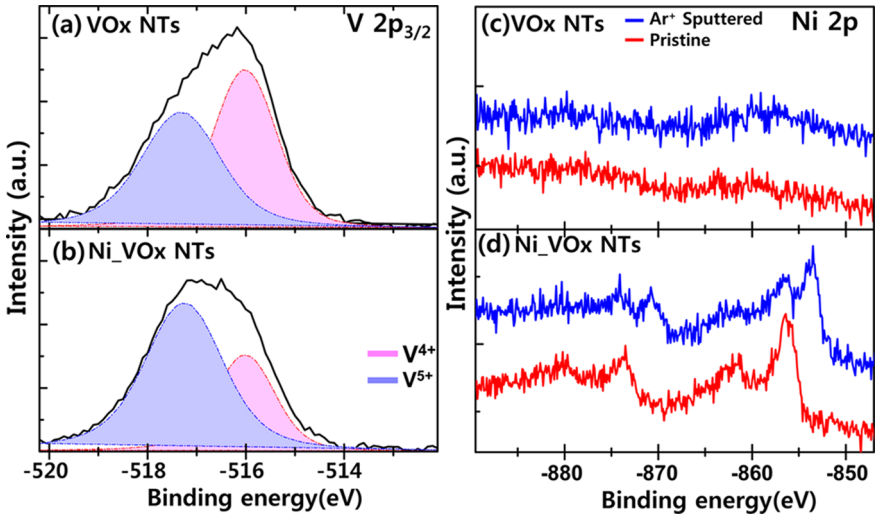

Figure 6. Core-level V $2p_{2/3}$ and Ni 2p spectra of (a, c) the VO_x NTs and (b, d) the Ni-doped VO_x NTs. The curve fits with the blue and red shaded areas in the V $2p_{2/3}$ spectra represent the V^{5+} and V^{4+} ion concentrations, respectively. The red and blue solid lines in the Ni 2p spectra present the VO_x NTs and the Ni-doped VO_x NTs in the pristine state and after being sputtered with Ar^+ ions, respectively.

result in higher potential in intercalation of Na ion. Figure 6c and d shows the Ni 2p core-level spectra for the VO_x NTs and the Ni-doped VO_x NTs, respectively. The spectra corresponding to the pristine state exhibited a peak at ~856 eV, which could be assigned to $Ni(OH)_2$ and/or Ni_2O_3. After etching using Ar^+ sputtering, the main peak appeared at ~853.4 eV and corresponded to NiO. The XPS results confirmed that some of the vanadium was oxidized during the cationic exchange reaction, resulting in greater potentials for Ni intercalation.

3. CONCLUSION

In this study, we successfully synthesized lamellar-structured VO_x NTs by a microwave-assisted hydrothermal method. Further, Ni was doped in between the VO_x layers by the cationic exchange method. The Ni-doped VO_x NTs exhibited enhanced initial electrochemical performance, that is, the initial capacity and rate performance of the Ni-doped VO_x NTs were significantly higher than that of the undoped VO_x NTs. These increases in the initial capacity and rate performance were attributed to the higher valence states of vanadium and higher electrical conductivity of VOx NTs being contributed to Na intercalation. In addition, it was confirmed that the interlayer spacing in the Ni-doped VO_x NTs increased after the insertion of Na ions during the intercalation process.

4. EXPERIMENTAL METHODS

4. 1. Synthesis of Nanotubes. Amounts of 0.91 g (0.05 mol) of V_2O_5 and 1.35 g (0.05 mol) of octadecylamine were stirred into 5 mL of ethanol for 1 h. Then, 15 mL of water was added to the solution. A homogeneous mixture was obtained after stirring using a magnetic bar for 48 h. This mixture was put in a Teflon-lined autoclave and heated at 180 °C for 18 h using a Mars 6 microwave. The final products were stirred in ethanol for 40 h to wash the residue and were subsequently filtered. The obtained VO_x powders were then heated in a convection oven at 80 °C for 12 h.

4. 2. Exchange Reaction. The Ni-doped VO_x NTs were obtained through a cationic exchange reaction. A total of 5.7 g of $NiCl_2$ was dissolved in 20 mL of deionized water. Then, 1 g of the synthesized VO_x NTs was dispersed in a solution of deionized water/absolute ethanol (volume ratio of 1/8), and the dispersion was stirred using a magnetic bar. Finally, the $NiCl_2$ solution and the dispersion of the VO_x NTs were mixed and stirred at 30 °C for 20 h. The final product was rinsed and filtered. The thus-obtained powder was dried in a vacuum oven at 80 °C for 12 h and then heated in the oven for 2 h.

4.3. Sample Characterization. The XRD analyses were performed using Cu Kα radiation for 2θ values ranging from 3° to 55°; the scan rate was 0.02° min^{-1}. The applied potential was 40 kV and current was 40 mA. XPS was performed using a Quantum 2000 Scanning ESCA Microprobe system (Physical Electronics Instruments). Focused monochromatized Al Kα radiation (1486.6 eV) was employed for the purpose. To avoid external contamination, all the samples were transferred in an Ar environment from the glovebox to the spectrometer using a transfer chamber. The morphologies of the VO_x NTs and the Ni-doped VO_x NTs were investigated using SEM (Hitachi S-4700N).

4.4. Electrochemical Measurements. The test cathodes were composed of 60 wt % active material, 20 wt % Ketjen black, and 20 wt % polyvinylidene difluoride. The composite was pasted on a piece of aluminum foil, which was used as the current collector. The cathodes were dried at 120° in vacuum and then pressed. Metallic Na was used as the anode. To synthesize the electrolyte, 1 mol L^{-1} $NaPF_6$ was dissolved in propylene carbonate. Glass fibers were used as the separator. R2032-type coin cells were assembled in an Ar-filled glovebox. Cyclic voltammetry (model VMP3, NanoQuébec) was performed at a scan rate of 10 μV s^{-1}. For the galvanostatic experiments, the cells were discharged/charged at a constant current.

■ ASSOCIATED CONTENT

Ⓢ Supporting Information

SAXS spectra of VOx NTs and Ni doped VOx NTs. This material is available free of charge via the Internet at http://pubs.acs.org/.

■ AUTHOR INFORMATION

Corresponding Author

*E-mail: ydmj79.park@samsung.com. Tel: +82-31-8061-1250. Fax: +82-31-8061-1319.

Notes

The authors declare no competing financial interest.

■ ACKNOWLEDGMENTS

This work was supported by the Samsung Advanced Institute of Technology.

REFERENCES

(1) Yabuuchi, N.; Kajiyama, M.; Iwatate, J.; Nishikawa, H.; Hitomi, S.; Okuyama, R.; Usui, R.; Yamada, Y.; Komaba, S. P2-type $Na_x[Fe_{1/2}Mn_{1/2}]O_2$ Made from Earth-Abundant Elements for Rechargeable Na Batteries. *Nat. Mater.* **2012**, *11*, 512−517.

(2) Palomares, V.; Serras, P.; Villaluenga, I.; Hueso, K. B.; Carretero-González, J.; Teófilo, R. Na-ion Batteries, Recent Advances and Present Challenges to Become Low Cost Energy Storage System. *Energy Environ. Sci.* **2012**, *5*, 5884−5901.

(3) Komba, S.; Takei, C.; Nakayama, T.; Ogata, A.; Yabuuchi, N. Electrochemical Intercalation Activity of Layered $NaCrO_2$ vs. $LiCrO_2$. *Electrochem. Commun.* **2012**, *12*, 355−358.

(4) Hosono, E.; Saito, T.; Hoshino, J.; Okubo, M.; Saito, Y.; Nishio-Hamane, D.; Kudo, T.; Zhou, H. High Power Na-ion Rechargeable Battery with Single-Crystalline $Na_{0.44}MnO_2$ Nanowire Electrode. *J. Power Sources* **2012**, *217*, 43−46.

(5) Berthelot, R.; Carlier, D.; Delmas, C. Electrochemical Investigation of the P2-Na_xCoO_2 Phase Diagram. *Nat. Mater.* **2011**, *10*, 74−80.

(6) Barpanda, P.; Lu, J.; Ye, T.; Kajiyama, M.; Chung, S. C.; Yabuuchi, N.; Komaba, S.; Yamada, A. A Layer-Structured $Na_2CoP_2O_7$ Pyrophosphate Cathode for Sodium-Ion Batteries. *RSC Adv.* **2013**, *3*, 3857−3860.

(7) Hamani, D.; Ati, M.; Tarascon, J. M.; Rozier, P. Na_xVO_2 as Possible Electrode for Na-Ion Batteries. *Electrochem. Commun.* **2011**, *13*, 938−941.

(8) Tepavcevic, S.; Xiong, H.; Stamenkovic, V. R.; Zuo, X.; Balasubramania, M.; Prakapenka, V. B.; Johnson, C. S.; Rajh, T. Nanostructured Bilayered Vanadium Oxide Electrodes for Rechargeable Sodium-Ion Batteries. *ACS Nano* **2012**, *6*, 530−538.

(9) Su, D.; Wang, G. Single-Crystalline Bilayered V_2O_5 Nanobelts for High-Capacity Sodium-Ion Batteries. *ACS Nano* **2013**, *7*, 11218−11226.

(10) Rui, X.; Lu, Z.; Yu, H.; Yang, D.; Hng, H. H.; Lim, T. M.; Yan, Q. Ultrathin V_2O_5 Nanosheet Cathodes: Realizing Ultrafast Reversible Lithium Storage. *Nanoscale* **2013**, *5*, 556−560.

(11) Lee, J. W.; Lim, S. Y.; Jeong, H. M.; Hwang, T. H.; Kang, J. K.; Choi, J. W. Extremely Stable Cycling of Ultra-Thin V_2O_5 Nanowire-Graphene Electrodes for Lithium Rechargeable Battery Cathodes. *Energy Environ. Sci.* **2012**, *5*, 9889−9894.

(12) Qu, Q.; Zhu, Y.; Gao, X.; Wu, Y. Core - Shell Structure of Polypyrrole Grown on V_2O_5 Nanoribbon as High Performance Anode Material for Supercapacitors. *Adv. Energy Mater.* **2012**, *2*, 950−955.

(13) Jiao, L.; Yuan, H.; Wang, Y.; Cao, J.; Wang, Y. Mg Intercalation Properties into Open-Ended Vanadium Oxide Nanotubes. *Electrochem. Commun.* **2005**, *7* (4), 431−436.

(14) Zhou, X.; Wu, G.; Gao, G.; Wang, J.; Yang, H.; Wu, J.; Shen, J.; Zhou, B.; Zhang, Z. Electrochemical Performance Improvement of Vanadium Oxide Nanotubes as Cathode Materials for Lithium Ion Batteries through Ferric Ion Exchange Technique. *J. Phys. Chem. C* **2012**, *116*, 21685−21692.

(15) Vera-Robles, L. I.; Naab, F. U.; Campero, A.; Duggan, J. L.; McDaniel, F. D. Metal Cations Inserted in Vanadium-Oxide Nanotubes. *Nucl. Instrum. Methods Phys. Res., Sect. B* **2007**, *261* (1), 534−1537.

(16) Reinoso, J. M.; Muhr, H. J.; Krumeich, F.; Bieri, F.; Nesper, R. Controlled Uptake and Release of Metal Cations by Vanadium Oxide Nanotubes. *Helv. Chim. Acta* **2000**, *83*, 1724−1733.

(17) Nordlinder, S.; Lindgren, J.; Gustafsson, T.; Edström, K. The Structure and Electrochemical Performance of Na^+-, K^+-, and Ca^{2+}-Vanadium Oxide Nanotubes. *J. Electrochem. Soc.* **2003**, *150* (5), E280−E284.

(18) Nordlinder, S.; Edström, K.; Gustafsson, T. The Performance of Vanadium Oxide Nanorolls as Cathode Material in a Rechargeable Lithium Battery. *Electrochem. Solid-State Lett.* **2001**, *4*, A129−A131.

(19) Wörle, M.; Krumeich, F.; Bieri, F.; Muhr, H. J.; Nesper, R. Flexible V_7O_{16} Layers as the Common Structural Element of Vanadium Oxide Nanotubes and a New Crystalline Vanadate. *Z. Anorg. Allg. Chem.* **2002**, *628*, 2778−2784.

(20) Liu, X.; Xie, G.; Huang, C.; Xu, Q.; Zhang, Y.; Luo, Y. A Facile Method for Preparing VO2 Nanobelts. *Mater. Lett.* **2008**, *62*, 1878−1880.